Flow-induced pressure fluctuations of a moderate Reynolds number jet interacting with a tangential flat plate

Alessandro Di Marco[*], Matteo Mancinelli[a] and Roberto Camussi[b]

Department of Engineering, University Roma TRE, Via Vito Volterra 62, 00146 Rome, Italy

Abstract.   The increase of air traffic volume has brought an increasing amount of issues related to carbon and NOx emissions and noise pollution. Aircraft manufacturers are concentrating their efforts to develop technologies to increase aircraft efficiency and consequently to reduce pollutant discharge and noise emission. Ultra High By-Pass Ratio engine concepts provide reduction of fuel consumption and noise emission thanks to a decrease of the jet velocity exhausting from the engine nozzles. In order to keep same thrust, mass flow and therefore section of fan/nacelle diameter should be increased to compensate velocity reduction. Such feature will lead to close-coupled architectures for engine installation under the wing. A strong jet-wing interaction resulting in a change of turbulent mixing in the aeroacoustic field as well as noise enhancement due to reflection phenomena are therefore expected. On the other hand, pressure fluctuations on the wing as well as on the fuselage represent the forcing loads, which stress panels causing vibrations. Some of these vibrations are re-emitted in the aeroacoustic field as vibration noise, some of them are transmitted in the cockpit as interior noise. In the present work, the interaction between a jet and wing or fuselage is reproduced by a flat surface tangential to an incompressible jet at different radial distances from the nozzle axis. The change in the aerodynamic field due to the presence of the rigid plate was studied by hot wire anemometric measurements, which provided a characterization of mean and fluctuating velocity fields in the jet plume. Pressure fluctuations acting on the flat plate were studied by cavity-mounted microphones which provided point-wise measurements in stream-wise and spanwise directions. Statistical description of velocity and wall pressure fields are determined in terms of Fourier-domain quantities. Scaling laws for pressure auto-spectra and coherence functions are also presented.

Keywords: turbulent jet; flat-plate; Corcos model; pressure spectra

1. Introduction

The development of air transport technology, primarily driven towards improving flight efficiency, has brought a dramatic increase in air traffic volume and consequent strong concerns from airport neighboring communities, mainly related to noise and pollution annoyances. Therefore, noise regulations have become stricter and noise characteristics more of a driving factor in aircraft engine design. The motivation for this study is related to the importance that this subject

---

∗Corresponding author, Research Assistant, E-mail: alessandro.dimarco@uniroma3.it
[a]Ph.D. Student, E-mail: matteo.mancinelli@uniroma3.it
[b]Professor, E-mail: roberto.camussi@uniroma3.it

has in aeronautical applications. Indeed, for most aircraft, the engine exhaust jet is typically a dominant noise source at take-off. During cruise, the engine noise impinges on the fuselage and is transmitted into the aircraft interior. The nozzle exhaust is in the close vicinity of the wing causing a strong aeroacoustic interaction. The exterior pressure field acting on the wing or eventually on the fuselage will be strongly influenced by the near field pressure fluctuations induced by the jet engine. Therefore, quantitative information regarding the levels of wall-pressure fluctuations are essential for attaining good engineering design and noise reduction methodologies, as the pressure field defines the forcing function which is used as input for the calculation of transmission loss through the fuselage sidewall.

A comprehensive study of four elementary jet-flat plate configurations was made to approach the problem. A moderate Reynolds number incompressible jet exhausting from a simple converging nozzle was set with the nozzle axis parallel to an instrumented flat plate. The flow was firstly aerodynamically characterized by means of hot wire velocity measurements. Then the effect of the flat plate presence was studied analyzing both the velocity field and the induced wall pressure fluctuations on the wall. The wall pressure fluctuations were acquired with an array of spatially separated microphones. Velocity and pressure measurements were taken with the flat plate installed at different radial distances from the nozzle axis and varying the axial position of the probe and array from the nozzle exhaust. More details are given in the following sections.

The article commences with a description of the experimental set-up and all the data concerning the acquisition instrumentation. The treatment of the pressure data is the specific argument of Section 4. The last section presents the conclusions of the investigation.

2. Experimental set-up

The experiments were carried out in the Aerodynamic and Thermo Fluid Dynamic Laboratory of the University Roma TRE. The subsonic/incompressible jet measurements were performed in a free-jet facility, which reproduces the facility developed by Chatellier *et al.* (2005) at the Trinity College of Dublin. A scheme of the jet apparatus is shown in Fig. 1.

A centrifugal blower exhausted through a wide angle diffuser into a cubic settling chamber which contained both honeycomb and screens. The ratio of the stream-wise length to single cell hydraulic diameter of the honeycomb as well as the porosity of the turbulence screens was designed to obtain the desired flow quality in terms of velocity profiles and turbulence intensity. Air flows into the inlet of a nozzle with an exit diameter of D=52 mm. To produce a uniform velocity distribution over a short length a smoothly contracting nozzle of $\approx$15 polynomial design contraction was used. The nozzle ends with a short round duct with a razor-sharp exit edge. The exhaust velocity was controlled adjusting the frequency of an asynchronous electric motor driven by an inverter, which moves the blower.

The jet issues in a large room in order to avoid disturbances or recirculation over the jet flow. The contraction ratio and the power of the motor enable the jet flow to achieve a maximum velocity at the nozzle exhaust (U_j) of around 50m/s corresponding to a maximum Mach number, M_j, of $\approx$0.15.

The measurements campaign presented in the next sections was carried out at U_j=42 m/s, corresponding to $Re\approx1.5\cdot10^5$, which classifies the jet as a moderate Reynolds number jet (Bogey *et al.*), and a Taylor Reynolds number $Re_T = <u'^2>^{1/2} \lambda_T / \nu \approx 382$, where λ_T is the Taylor micro-scale and u' is the turbulent fluctuating velocity.
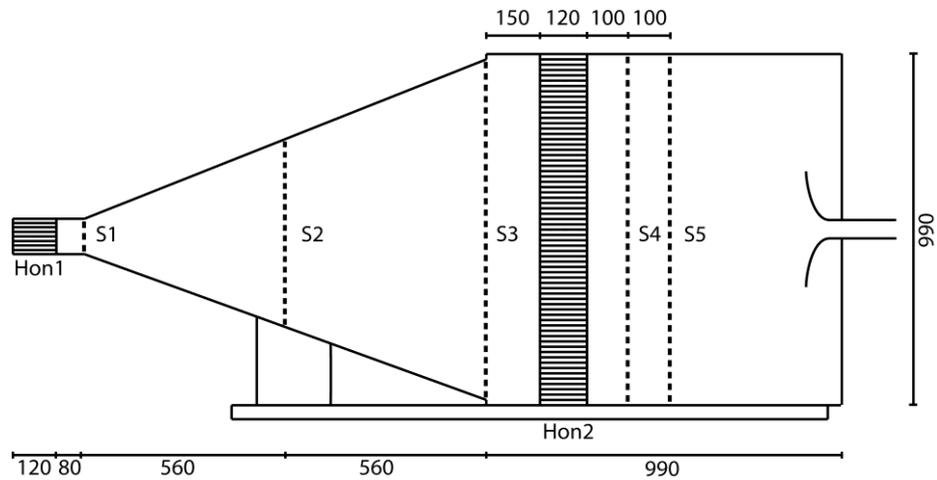
Fig. 1 Layout of the experimental free jet facility. The measures are in millimeters. The abbreviation Hon# indicates the honeycomb and S# the turbulence screen
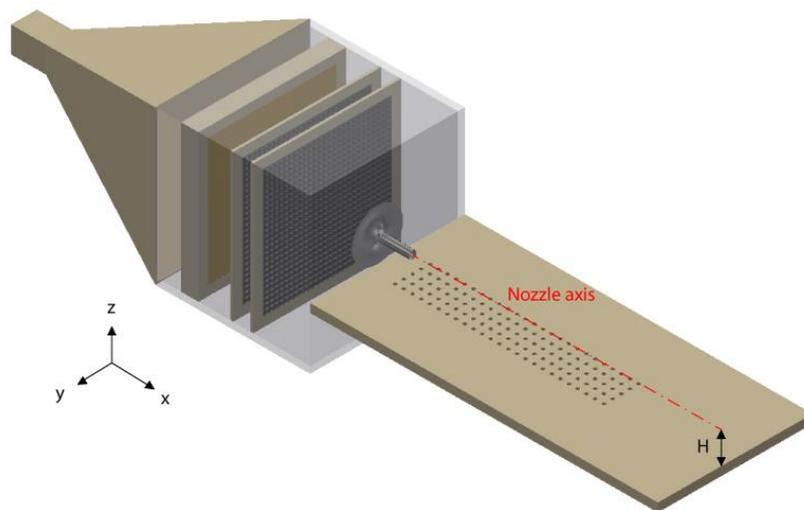

Fig. 2 Scheme of the pin-holes distribution on the flat plate and identification of the reference system. The parameter H represents the distance between the flat plate and the nozzle axis.

In order to pursue the objectives of the work, a rigid flat plate representing the airframe model was placed parallel to the nozzle axis. A schematic representation of the set-up and the reference frame adopted is provided in Fig. 2. The flat plate was installed on a rigid traverse structure facilitating the accurate positioning in the direction perpendicular to the plate itself (z-axis) and allowing small rotation angles along the x- and y-direction in order to align the surface to the flow direction. The size and material of the flat plate were chosen to avoid border effects and to obtain an optimal stiffness. The precise radial distance (H) and alignment of the flat plate with respect to the nozzle axis (shown in Fig. 2) was carefully checked using a laser-levelling instrument.

Fig. 3 Scheme of the microphone cavity and the pinhole. The microphone is mounted through a properly designed connector. The pinhole diameter is 1.5 mm

3. Instrumentation

The aerodynamic behaviour of the free jet was characterized through velocity measurements performed with a hot wire anemometer system.

Jet flow velocity measurements were taken using a single sensor hot wire anemometer probe (DANTEC 55P11) of 1 mm in length and 5 μm in diameter. The hot wire probe was carefully mounted on a micro-metric traversing system. The traversing system consisted in one vertical rail spanning the length of interest and a sting used to hold the velocity instrumentation probe stem. The probe stem was carefully aligned with the y-direction and in bi-normal position to reduce flow disturbances and provide the accurate measurement of the axial velocity component (parallel to the *x*-direction).

The single wire system was operated by a constant temperature anemometer system (AN-1003 Lab-System). Hot wire anemometer signals were taken by a National Instruments acquisition system (PCI-6221). The sampling frequency was set to 100 kHz, the anti-aliasing low-pass filter frequency cut-off at 20 kHz and the acquisition time to 11 s. The frequency cut-off of the filter was chosen to maximize the resolution of the smallest scales.

The wall-pressure time-series studied in the current investigation were measured using three Microtech Gefell M360 electret microphones cavity mounted on an optimized pressure tap according to the scheme reported in Fig. 3. The characteristic dimensions of the cavity and pressure tap were properly designed in order to avoid the presence of the Helmholtz resonant peak in the measured frequency range. The pinhole diameter is 1.5 mm. The length of the neck is about 2 mm and the volume of the cavity of about $2.5 \cdot 10^{-8}$ mm^3.

The three-microphone array was mounted and moved over the grid of pressure taps shown in figure 2. Pressure taps were separated by 1D in the stream-wise and span-wise directions. The pressure signals were acquired by a National Instruments acquisition system (SCXI-1600) with a sampling frequency set to 40 kHz, an anti-aliasing low-pass filter frequency cut-off at 20 kHz, and for an acquisition time of 10 s.
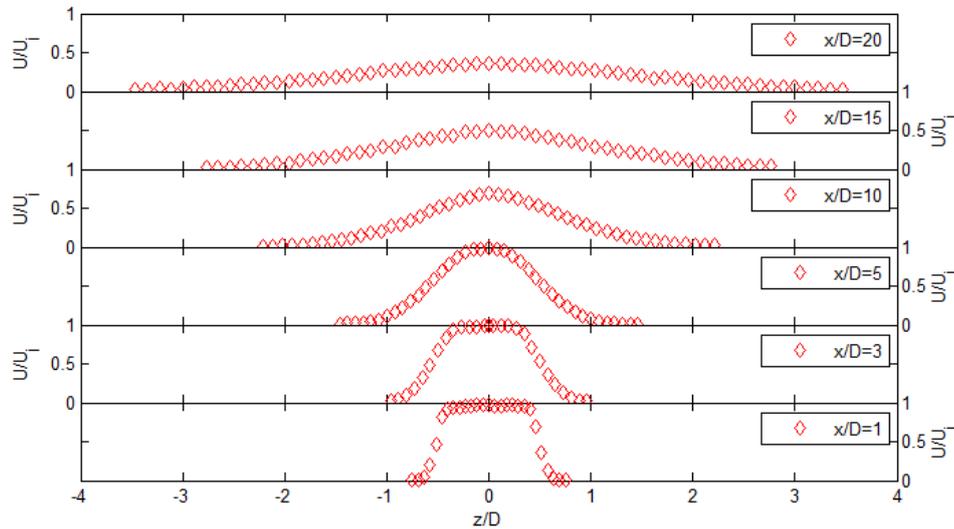
Fig. 4 Stream-wise mean velocity at different axial positions.

In order to characterize the overall effect of the jet flow on the wall pressure intensity, mean pressure measurements were conducted as well. The above described pressure taps were connected to a pressure transducer (Kavlico P592) through a transmission line designed to fit the different diameters of the inlet port and the pressure tap. Mean wall pressures were acquired for 10 s with a sampling frequency of 1 kHz.

4. Presentation and discussion of results

4.1 Free jet characteristics

From the measured data sets, a first characterization of the jet aerodynamics is performed. The mean axial velocities, normalized by the velocity at the nozzle exhaust, at different axial positions *x/D* are presented in Fig. 4. The profiles are symmetric and the top hat distribution at the nozzle exit tends to persist to about 5-6D.

The corresponding axial turbulence intensity profiles are displayed in Fig. 5. The location of the peaks in the turbulence intensity profile corresponds to the local maximum of the mean velocity gradient.

Typical Power Spectral Densities obtained at various axial positions are plotted in Fig. 6 in dimensionless form. The PSD amplitude normalized by the square of U_j are represented as a function of the Strouhal number $St_D=fD/U_j$. Spectra exhibit a peak around $St_D=0.46$ for $x/D{\leq}4$ which is the mark of large-scale structures caused by a shear layer instability of Kelvin-Helmholtz type. As the axial position increases, after a transition region, the self-similarity condition is reached and the flow becomes fully turbulent at about $x/D \geq 15$ where a relatively extended inertial range (about one decade) is evidenced by the comparison with the Kolmogorov power law $St^{-5/3}$ (Kolmogorov 1941).
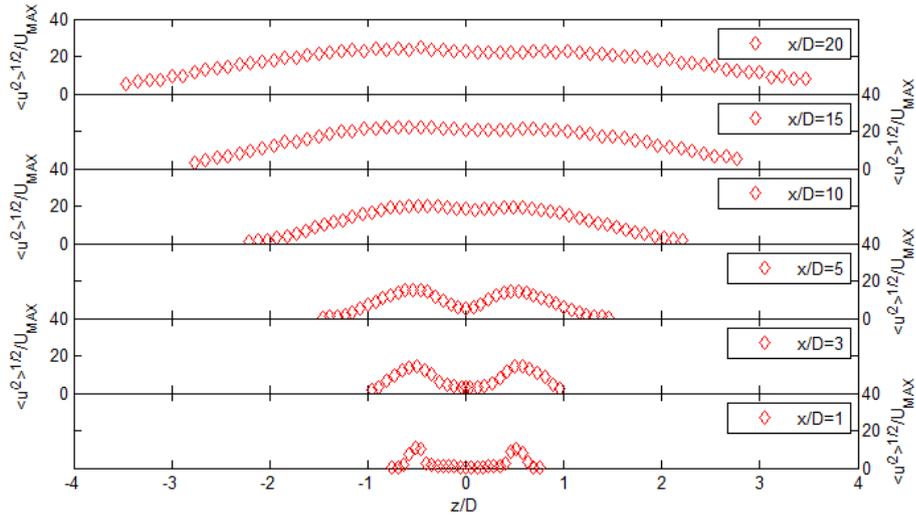
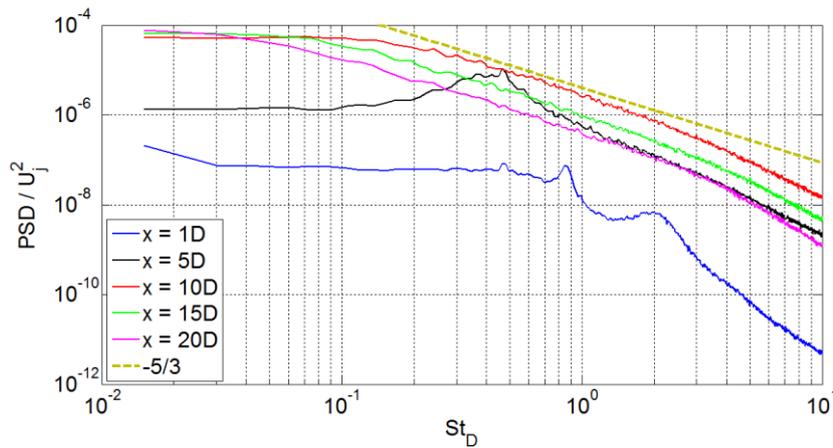Fig. 5 Stream-wise turbulence intensity at different axial positions.

Fig. 6 Axial evolution of dimensionless velocity power spectra vs Strouhal number.

4.2 Wall pressure spectra

Wall pressure fluctuations were measured along the flat plate at four radial distances: H/D=1, 1.5, 2 and 2.5. The array of three Gefell microphones was moved for each radial distance in stream-wise and span-wise directions in order to map the signature of the jet on the surface. The spatial grid over which the microphone array was moved is shown in Fig. 2. The Sound-Pressure Spectrum Levels (SPSL) (Pierce 1989) of the stream-wise evolution as a function of the Strouhal number St_D obtained for each radial distance are shown in Fig. 7. The reference pressure used in the following calculations is 20 μPa.

The sound pressure levels and the spectral shape in Fig. 7 change significantly as the jet-flat plate separation distance increases. Such a behavior is particularly detectable for small axial
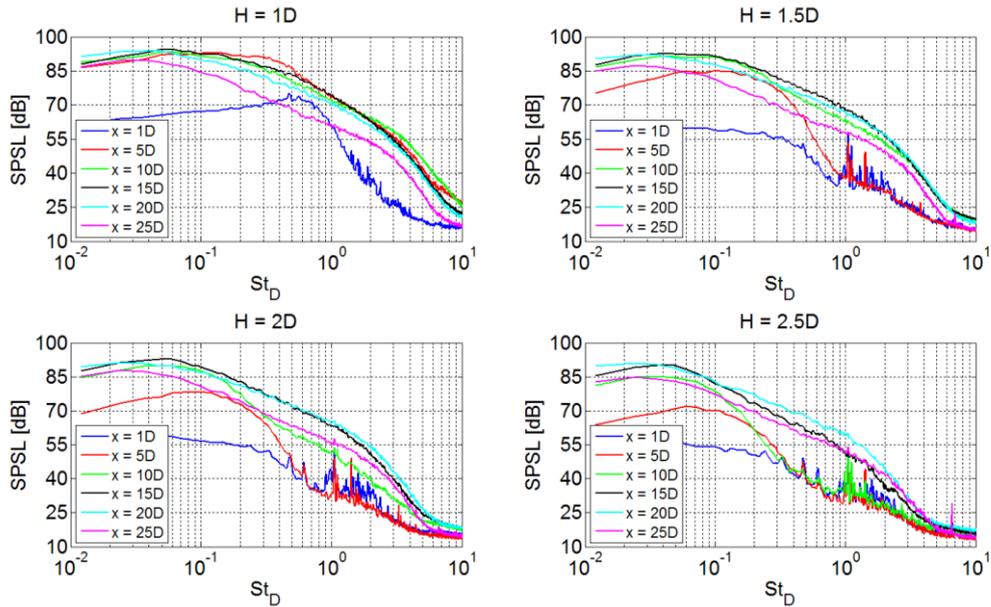
Fig. 7 Stream-wise SPSL evolution for *y/D*=0 at *H/D*=1, *H/D*=1.5, *H/D*=2 and *H/D*=2.5
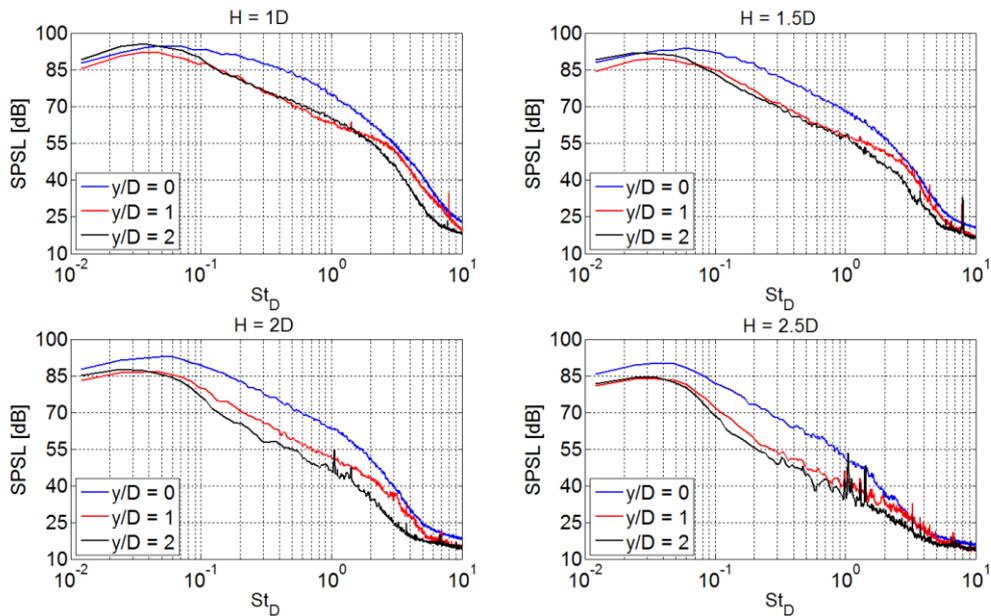

Fig. 8 Span-wise SPSL for *x/D*=15 at *H/D*=1, *H/D*=1.5, *H/D*=2 and *H/D*=2.5

distances and for the surface position closer to the jet, where the spectra show a higher energy content over the whole frequency range. As the axial distance increases, the energy of the fluctuating pressure increases and the shape of the spectra changes accordingly. This is due to the relationship between the radial position of the plate and the axial location where the jet hits the
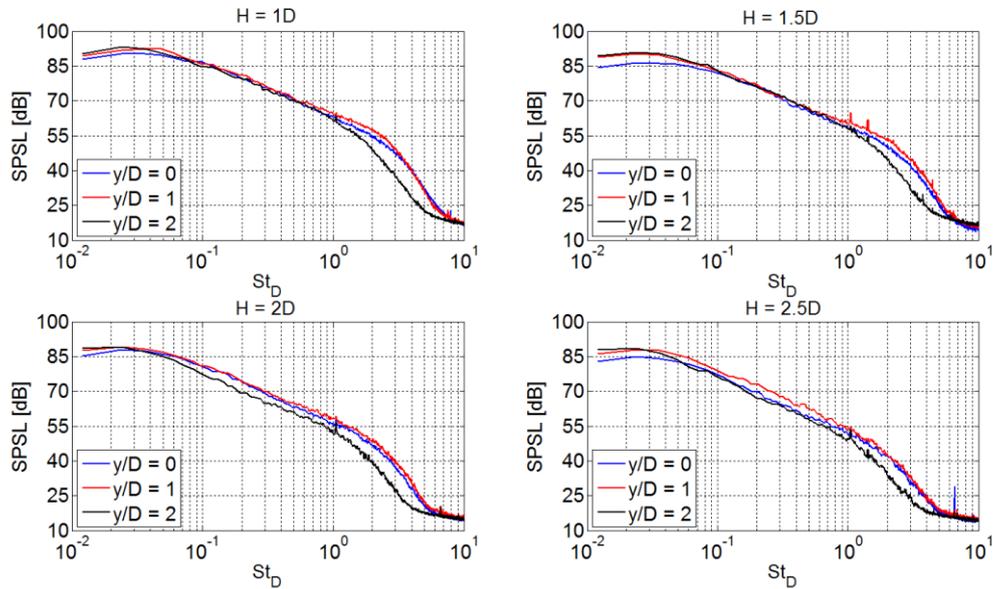
Fig. 9 Span-wise SPSL for *x/D*=25 at *H/D*=1, *H/D*=1.5, *H/D*=2 and *H/D*=2.5

surface. The wall pressure statistics also changes significantly if the impact occurs correspondingly to the potential core region, the transition region or the fully developed region of the jet. A quasi-equilibrium turbulent boundary layer (TBL) on the surface can be established only at large distances from the impact region, this behavior being again related to the radial position of the flat plate. The Sound-Pressure Spectrum Levels (SPSL) of the span-wise evolution as a function of the Strouhal number St_D obtained for each radial distance are shown in Fig. 8 and Fig. 9 for axial positions *x/D*=15 and *x/D*=25 respectively.

Spectra show a higher energy content in the mid frequency range at *y/D*=0 and *x/D*=15 and tend to collapse as the axial position approaches a corresponding fully turbulent jet region. For the high frequency range even farther from the nozzle exhaust the energy content of the span-wise position *y/D*=2 is always significantly lower than *y/D*=0 and 1.

The spectrum behavior in the mid-high frequencies for lower stream-wise separations is due to the background noise induced by the fan.

4.3 Wall pressure spectra scaling

The scaling behavior of the wall pressure spectra can be used to link spectral features with their respective governing variables. At high frequencies, the roll off region has been associated with the inner portion variables of the boundary layer. The low frequency part of the spectrum, found just before the so called overlap region, has been associated with the outer portions of the turbulent boundary layer, while the mid frequency region has been linked to the logarithmic layer in the boundary layer (Farabee 1991, Goody 2004, Gravante *et al.* 1998). It has to be pointed out that in the case under investigation the wall pressure fluctuations do not properly correspond to those of a typical TBL being generated by the acoustic and the hydrodynamic interaction of a jet flow and a tangential flat plate at various radial distances. For large x/D, after the impact zone and where the
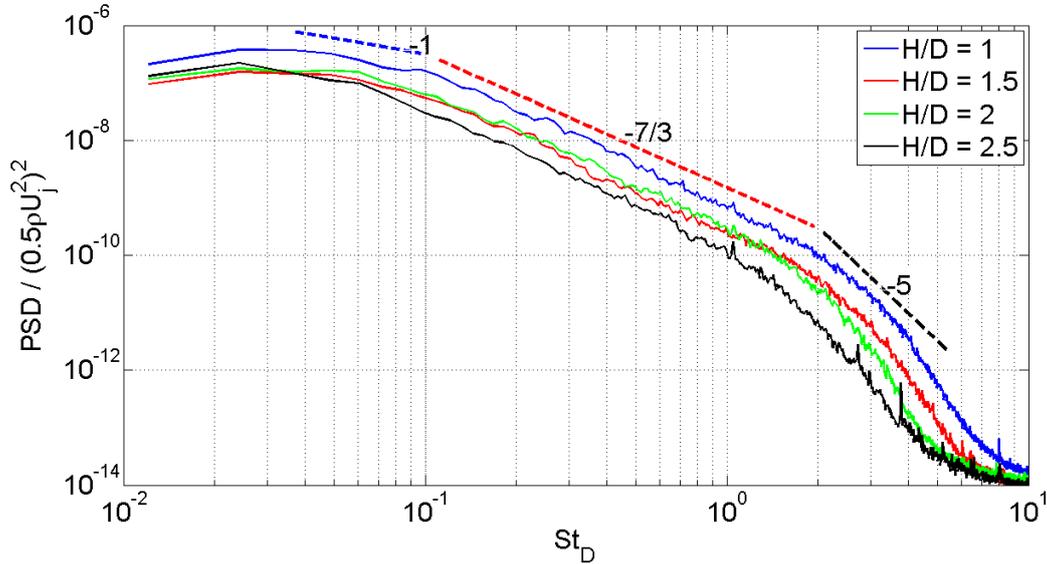
Fig. 10 Dimensionless PSDs at *x/D*=25 for the flat plate distances considered

jet flow has sufficiently developed over the flat plate, a universal trend similar to the effect of a TBL development over a wall (Hwang *et al.* 2009) can be found. The wall pressure spectra divided by the dynamic pressure as a function of St_D at the maximum axial position and for all the radial distances *H/D* are shown in Fig. 10.

The overlap region in the low-mid frequency range exhibits an f^{-1} dependency according to the commonly observed energy decay law due to the turbulence activity located in the logarithmic region of a fully developed TBL. In the mid frequency range an $f^{-7/3}$ decay power law applies well. This region has been linked to pressure sources from the boundary layer buffer region (Gravante *et al.* 1998).

Beyond this buffer region at the highest frequencies of the roll off region where the spectral shape is influenced by flow viscosity, an f^{-5} slope is typically expected. The present data show a good agreement with the literature predictions. Due to the complex structure of the flow investing the flat plate and its dependence on the different geometrical configurations considered, it was not possible to obtain a single scaling law, which leads to a satisfactory collapse of all the experimental spectra. A scaling criterion based on outer variables at axial distances sufficiently far from the impact zone is proposed. The inner variable scaling at high frequencies has not been applied. More details regarding the boundary layer behavior should be needed, but this was not the topic of the present experimental campaign. The main parameters influencing the aerodynamic behavior of the wall pressure fluctuations were chosen as scaling variables. The frequency was scaled using *H* as a reference length and U_j as a reference velocity defining the Strouhal number $St_H=fH/U_j$. The amplitude of the pressure spectrum was scaled through the dynamic pressure based on the convection velocity U_c and choosing a time scale related to the time occurring to a fluid particle advected by the mean flow to reach the flat plate. That was estimated by the ratio H/U_c. The convection velocity was calculated as the ratio between the microphone distance and the time lag at which the cross-correlation maximum is found. The scaled pressure spectra are presented in Fig. 11.
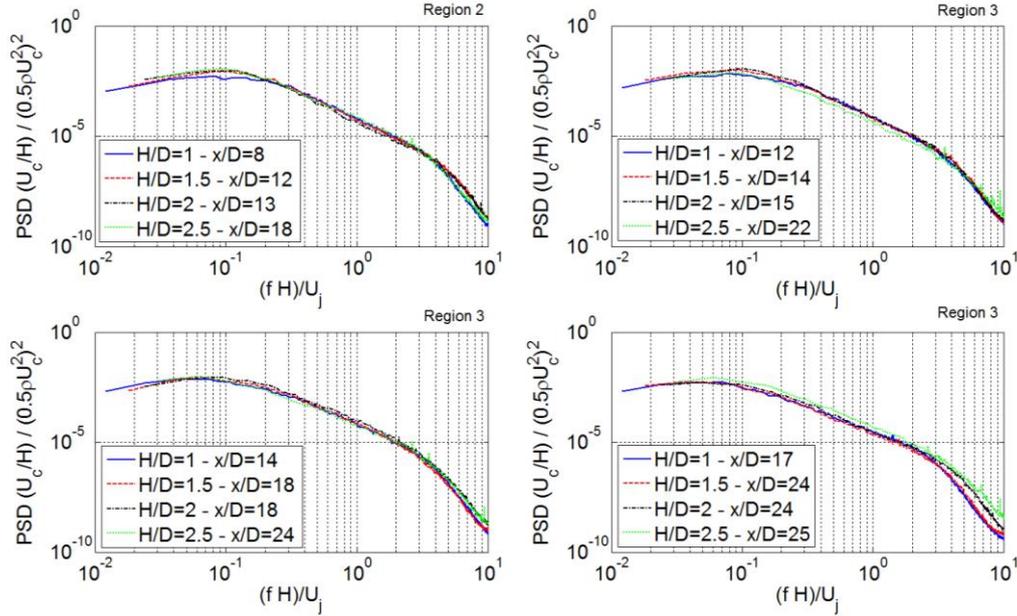
Fig. 11 Scaled spectra using outer variables as function of the flow evolution on the flat plate. For more details on the region definition, the reader is referred to Di Marco *et al.* (2015)

The spectra in each plot are grouped in regions depending upon the flow evolution over the flat plate as well as the radial distance. The flow evolution is a function of the radial distance. It has to be pointed out that all the axial positions in the plot are chosen far away from the impact zone. Mean pressure measurements made with the Kavlico pressure transducers helped in the determination of the different regions over the flat plate. The corresponding analysis is not reported here for the sake of conciseness. More details are given in Di Marco *et al.* (2015). The results show a good collapse at low and mid frequencies indicating that the spectra reach a universal behavior before the TBL becomes fully developed.

4.4 Wall pressure coherence and modeling

Additional information about the evolution or the decay of the pressure field can be obtained by the analysis of the coherence function, a non-dimensional and real quantity format of the cross-spectrum, which is evaluated as follows (Farabee *et al.* 1991)

$$\gamma(\xi, \omega) = \frac{|\Phi_{p_1 p_2}(\xi, \omega)|}{[\Phi_{p_1}(\omega)\Phi_{p_2}(\omega)]^{1/2}}, \tag{1}$$

where ω is the angular frequency, $\phi_{p_1 p_2}$ the cross-spectrum, ϕ_{p_1} and ϕ_{p_2} the auto-spectra of two consecutive microphones separated in the stream-wise direction by ξ varying from $1D$ to $2D$.

Based on the results summarized in Di Marco *et al.* (2015), the coherence function was calculated along the nozzle axis beyond the axial positions for which the jet impacts the flat plate. Although cross-spectral data were obtained in both directions only results from stream-wise data set will be presented.
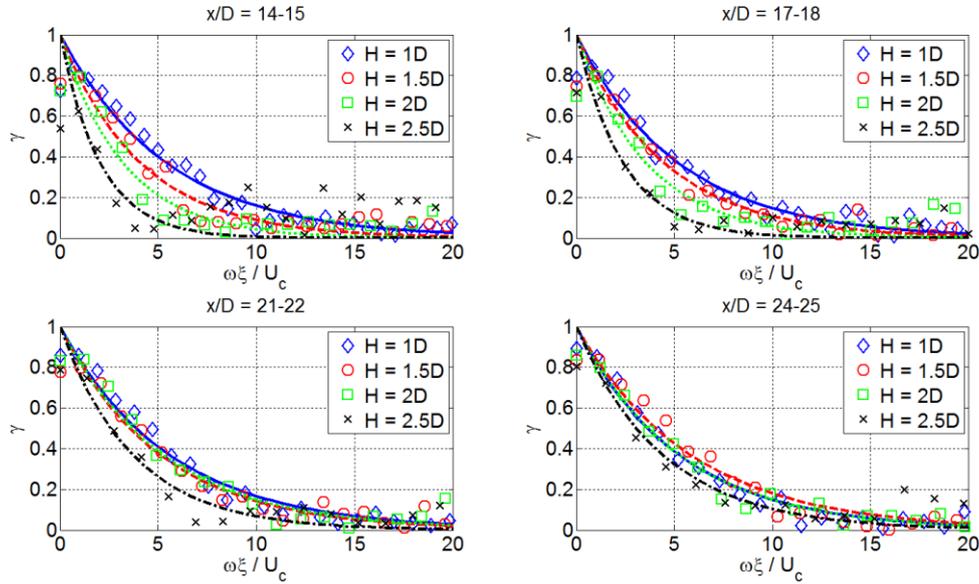
Fig. 12 Coherence functions and Corcos' model fits parametrized by the flat plate distance for different axial positions beyond the impact point

Experimental results were compared with the coherence decay function proposed by Corcos (1962, 1963). The prediction model is defined as follows

$$\gamma(\xi, \omega) = e^{\left(-\alpha \frac{\omega \xi}{U_c}\right)}, \qquad (2)$$

where the decay rate constant α was determined by applying a least mean square optimization algorithm to the experimental data and U_c, the convection velocity, was computed from the time delay corresponding to the peak of the cross-correlation function between pairs of microphones in the stream-wise direction.

The wall pressure spectrum coherence for a stream-wise separation $\xi=1D$ versus the phase angle $\omega\xi/U_c$ (Farabee *et al.* 1991) are shown in Fig. 12.

The coherence functions are plotted for fixed axial positions and varying the radial distance of the flat plate. All the axial positions are far away from the impact point, i.e., $x/D\geq13$. The Corcos' model well reproduces the exponential decay for each configuration considered. At axial positions close to the $x/D=14-17$ zone the decay rate growths as the radial distance of the flat plate is increased and some discrepancies at $H/D=2.5$ for the highest frequencies are found. At axial positions close to the $x/D=21-25$ zone where the flow over the flat plate is approaching a developed TBL condition, the experimental points become less scattered and tends to collapse for all the flat plate distances. This behavior is confirmed by inspecting Fig. 13. The figure shows the axial evolution of the coherence function along the nozzle axis for each radial distance. It can be observed that the exponential decay is well reproduced, but the decay coefficient decreases for increasing distances x/D.

Fig. 14 summarizes the axial evolution of the Corcos' coefficient for all H/D compared with the range values found in the literature (see e.g., Bull 1967, Brooks *et al.* 1981). The decay rate in
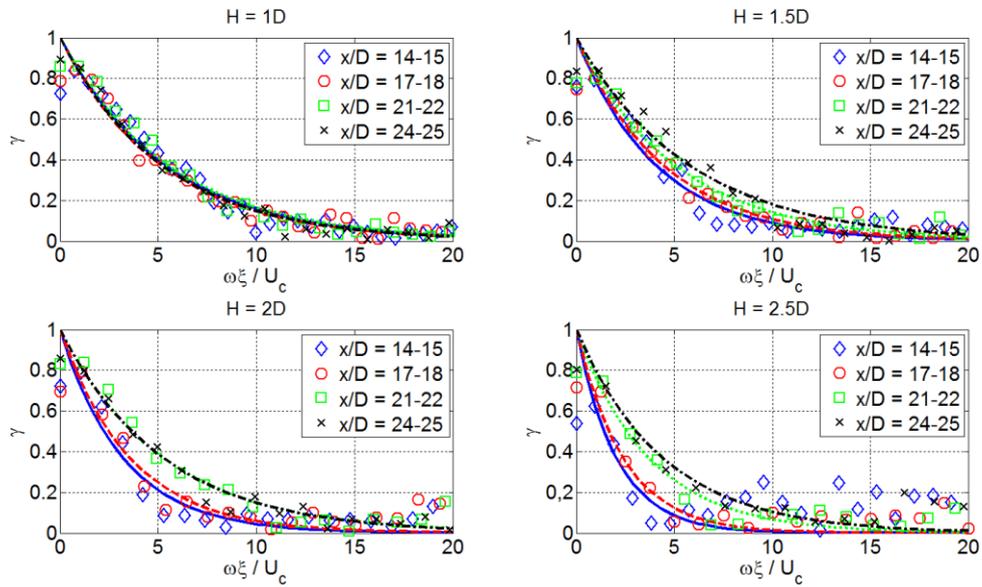
Fig. 13 Stream-wise evolution of the coherence function for all the flat plate radial distances
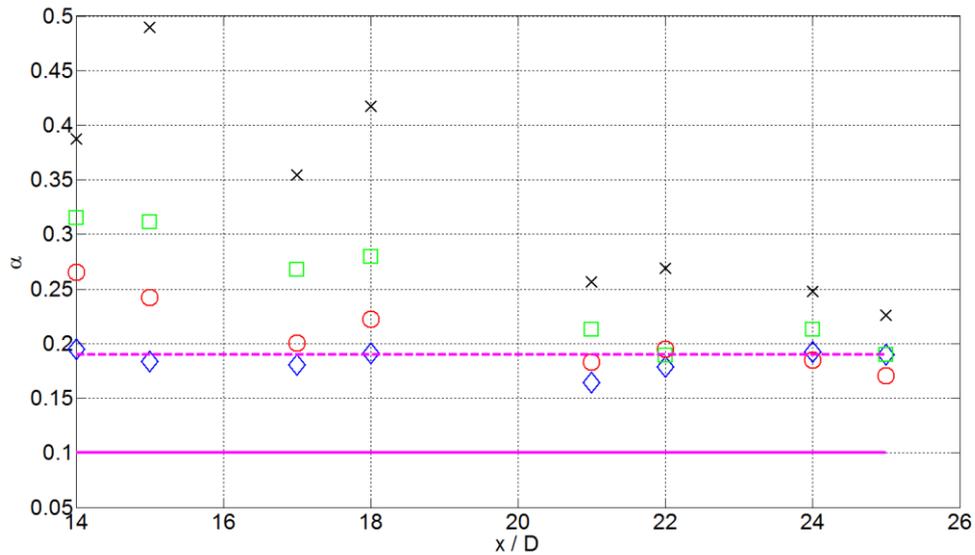

Fig. 14 Axial evolution of the Corcos' model stream-wise coefficient from x/D=14 to x/D=25 for flat plate distances: ◇ H/D=1; ○ H/D=1.5; □ H/D=2; × H/D=2.5. Solid line and dashed line refers respectively to the lower and upper limit values of the Corcos' model coefficient found in the literature

stream-wise direction is typically found in the range spanning from 0.1 to 0.19.

For the smallest H/D it is found $\alpha \simeq 0.2$ that is surprisingly in very good agreement with the amplitude reported in the literature for equilibrium TBLs. At larger H/D, the measured Corcos'

coefficients are higher than those found in the literature. The larger is *H/D* the larger is the coefficient. Fixed a radial distance *H/D*=2 and 2.5, for increasing *x/D* the amplitude of α decreases and the trend is to reach the amplitude 0.2, expected for equilibrium TBLs.

The coherence spectra for two stream-wise separation spacing ξ=1*D* and ξ=2*D* at all the flat plate radial distances are displayed in figure 15 and figure 16 at axial positions *x/D*=13 and *x/D*=23 respectively. The Corcos' model fitted on the spatial separation is displayed as well.
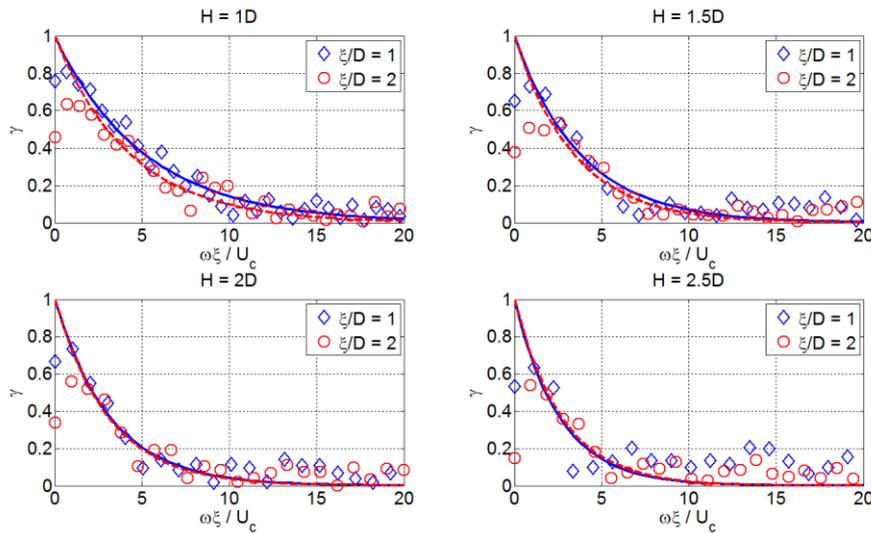

Fig. 15 Streamwise coherence and Corcos' model versus cross-spectral phase for 2 spacings ξ=1−2*D* at *x/D*=13 for all the flat plate radial distances
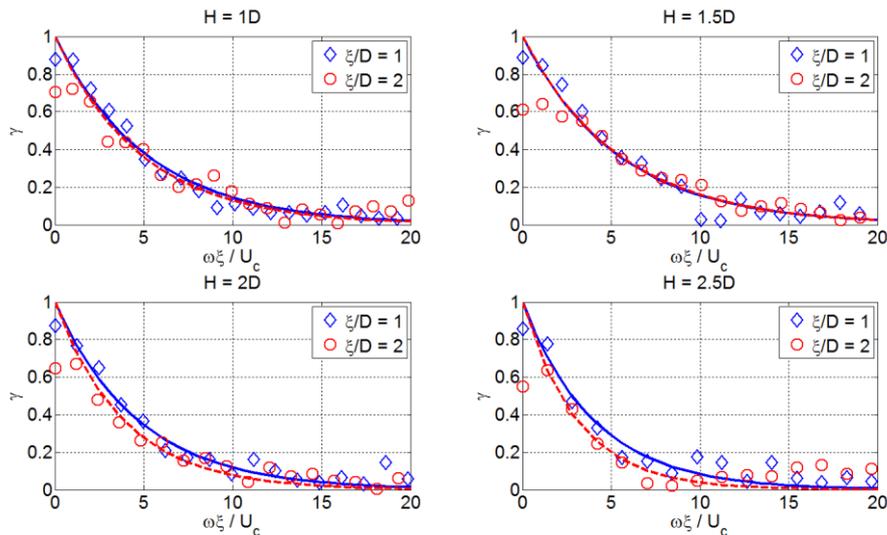

Fig. 16 Streamwise coherence and Corcos' model versus cross-spectral phase for 2 spacings ξ=1−2*D* at *x/D*=23 for all the flat plate radial distances

The large coherence values found at low frequencies suggest that the larger turbulent eddies responsible for low frequency signals have a longer persistence over the distances analyzed than the smaller, higher frequency eddies, similar to what was found in Farabee *et al.* (1991).

At the axial position *x/D*=13 the coherence collapse for small radial distances is well verified. As the radial distance increases, depending upon the flow evolution over the flat plate, the high frequency portion of each coherence spectrum deviates above a universal curve modeled using the Corcos' formulation. This high frequency behavior demonstrates that the flow has not completely developed. Indeed, at higher axial positions such those shown in Fig. 16 where the flow approaches or is going to approach a fully developed TBL, the curves tend to collapse to a universal one excepted for the *H/D*=2.5 radial distance, probably still needing more space.

5. Conclusions

The interaction between an incompressible moderate Reynolds number jet with a tangential flat plate has been investigated.

The aerodynamic characterization of the jet in free conditions was first provided by hot wire anemometer measurements at different axial positions moving the probe along the *z*-axis. Axial evolution of mean and fluctuating velocity profiles has been shown.

Hot wire anemometer measurements and wall pressure measurements were carried out in order to characterize the jet-surface interaction. The present work focused on the analysis of the wall pressure fluctuation field acting on a flat rigid surface in terms of its spectral content. The plate was located at different radial distances from the nozzle axis; pressure measurements were acquired by an array of three 1D-spaced microphones. The pressure spectra showed that the physics of the jet-surface interaction is strongly dependent on the radial position of the flat plate and the axial location considered. Indeed the position along the stream-wise direction for which the jet impinges on the surface changes significantly with the plate location with respect to the jet. Therefore, the energy content of the wall pressure fluctuations changes significantly as in terms of amplitude as in terms of spectral shape depending on the axial location and the plate distance from the jet considered. For low axial distances, the spectra referred to the flat plate radial positions close to the jet show a higher energy content. As the axial distance increases, the difference in terms of spectral shape between the spectra related to the different plate positions disappears. Downstream from the nozzle exhaust the spectra for all *H* exhibit energy decay laws typical of wall pressure fluctuations in turbulent boundary layers, such feature being the proof that a quasi-equilibrium TBL can be established. In the span-wise direction at low axial distances a significant difference in spectral content can be observed, the energy of the spectra along the jet axis being much higher than the one of the spectra for larger transverse positions. As axial distance increases such discrepancy disappears and the spectra almost collapse.

A scaling criterion for wall pressure spectra based on external aerodynamic variables and main geometrical length scales was derived. The scaling law applies for spectra at axial positions far from the nozzle exit so that the jet has impinged on the surface for all the flat plate positions, the axial position considered being dependent on the corresponding surface distance from the jet. The collapse was satisfactory.

Coherence functions of wall pressure spectra for all the plate radial distances were computed along the stream-wise direction for an axial position for which the jet had already impacted on the surface. The coherence showed an exponential decay against the phase angle velocity. Comparison

of the experimental data with the analytical Corcos' model was performed. The results showed that for *H/D=1* the values of the experimental Corcos' coefficient were the ones found in the literature for wall pressure in TBLs. For the other plate positions for low axial distances the coefficient values were a little higher than the ones predicted by Corcos; as axial distance increases and the flow develops over the surface the coefficients tend to the values of Corcos' model. A good collapse of the coherence functions parameterized by the separation ξ between the microphones was also found, especially for high axial distances. Such a behavior confirms again that downstream the nozzle exhaust the wall pressure fluctuations related to the jet-surface interaction approach the physics of a quasi-equilibrium turbulent boundary layer.

Acknowledgments

References

Bogey, C., Marsden, O. and Bailly, C. (2012), "Effects of moderate Reynolds numbers on subsonic round jets with highly disturbed nozzle-exit boundary layers", *Phys. Fluid.*, **24**, 105107.

Brooks, T.F. and Hodgson, T.H. (1981), "Trailing edge noise prediction from measured surface pressures", *J. Sound Vib.*, **78**(1), 69-117.

Bull, M.K. (1967), "Wall-pressure fluctuations associated with subsonic turbulent boundary layer flow", *J. Fluid Mech.*, **28**(4), 719-754.

Chatellier, L. and Fitzpatrick, J. (2005), "Spatio-temporal correlation analysis of turbulent flows using global and single-point measurements", *Exp. Fluid.*, **38**(5), 563-575.

Corcos, G. M. (1963), "Resolution of pressure in turbulence", *J. Acoust. Soc. Am.*, **35**, 192-199.

Corcos, G.M. (1962), "Pressure fluctuations in shear flows", Technical Report, **183**, University of California, Institute of Engineering Research Report Series.

Di Marco, A., Mancinelli, M. and Camussi. R. (2015), "Pressure and velocity measurements of an incompressible moderate Reynolds number jet interacting with a tangential flat plate", *J. Fluid Mech.*, **770**, 247-272.

Farabee, T.M. and Casarella, M.J. (1991), "Spectral features of wall pressure fluctuations beneath turbulent boundary layers", *Phys. Fluid.*, **3**(10), 2410-2420.

Finnveden, S., Birgersson, F., Ross, U. and Kremer, T. (2005), "A model of wall pressure correlation for prediction of turbulence-induced vibration", *J. Fluid. Struct.*, **20**(8), 1127-1143.

Goody, M. (2004), "Empirical spectral model of surface pressure fluctuations", *AIAA J.*, **24**(9) 1788-1974.

Gravante, S.P., Naguib, A.M., Wark, C.E. and Nagib H.M. (1998), "Characterization of the pressure fluctuations under a fully developed turbulent boundary layer", *AIAA J.*, **36**(10), 1808-1816.

Hwang, Y.F., Bonness, W.K. and Hambric S.A. (2009), "Comparison of semi-empirical models for turbulent boundary layer wall pressure spectra", *J. Sound Vib.*, **319**(1-2), 199-217.

Kolmogorov, A.N. (1941), "The local structure of turbulence in an incompressible fluid for very large Reynolds numbers", *Dokl. Akad. Nauk SSSR*, **30**(4), 301-305. Reprinted in *Proc. R. Soc. Lond A* **434**, 9-13.

Pierce, A.D. (1989), *Acoustics: An Introduction to Its Physical Principles and Applications*, Acoustical Society of America.